Fracture micromechanisms and mechanical behavior of YBCO bulk superconductors at 77 and 300 K

K. Konstantopoulou , J.J. Roa , E. Jiménez-Piqué , M. Segarra , J.Y. Pastor

Abstract

In this study two $YBa_2Cu_3O_{7-\delta}$ bulk superconductors were evaluated, with the aim of analyzing the influence of the processing method (TSMG and Bridgman) and the test temperature on their mechanical behavior. The relationship between their mechanical properties and fracture micromechanisms has also been studied. Both materials were tested at room and at service temperature. TPB tests were carried out to determine their mechanical behavior, strength and toughness. Moreover, one of the two materials, characterized by transversal microstructural anisotropy, was tested in two directions. Hardness of both materials at nano and micro scale was studied. The results show that the mechanical behavior of the materials is controlled by the defects and cracks that have been introduced during the processing of the materials. A good degree of agreement was found between the experimental crack defects detected by means of SEM and those gathered from the fracture mechanical analysis of the experimental data.

Keywords: YBaCuO; Mechanical behavior; Superconductors; Cryogenic; Microstructural defects

1. Introduction

The Second generation superconducting bulk materials show high critical current density and high trapped magnetic field at cryogenic temperatures, Tc. The development of these materials that present a superconducting behavior at temperatures above 77 K ($Tc \cong 92$ K) is of great technological and scientific interest.

$YBa_2Cu_3O_{7-\delta}$ (YBaCuO or Y-123) big melt-textured monoliths are highly attractive materials as permanent magnets. These materials are currently able to trap magnetic fields of over 1 T at 77 K and of 4 T at 50 K [1], which are temperatures that are easily reachable by actual cryocoolers.

Practical applications of these materials are often limited because of their poor mechanical performance, especially at cryogenic temperatures. For example, the field-trapping capability of melt-textured materials can be improved by enlarging the sample size; though this is not easily achieved since intense magnetic fields can produce strong magnetic forces, which can lead to complex stress fields generated by the flux density gradients that will in turn give rise to an undesired fracture of the material [2,3,4]. As a consequence, further improvements are limited by their current mechanical properties. Besides, YBaCuO materials are brittle ceramics, whose mechanical properties and maximum trapped fields, commonly tend to degrade due to weak regions in the microstructure such as cracks, which are inherent in the growth process and induce local stress concentrations and eventual cracking of the samples [5]. Furthermore, microcracks are always present in such materials, given the fact that they are associated with the stress induced in the superconducting matrix by the microstructure of the YBaCuO, while cooling down from the processing temperature, and also due to the oxygenation

process [6,7]. Therefore, the study of not only their macroscopical mechanical properties, but also their local mechanical properties is crucial for their industrial application.

These high temperature superconducting materials (HTSC) present an intrinsic anisotropy in its microstructure because of the perovskite structure [8]. For this reason, strength and toughness show a macroscopically anisotropic behavior. Hence, the study of their mechanical properties is a key point in achieving structural reliability. Moreover, optimization (mechanical and functional) is highly relevant for their potential applications as bulk high-temperature superconductors in generating large magnetic fields for a wide and attractive variety of applications, such as motors and permanent magnets, amongst others.

As a consequence of industrial requests, both low costs and high stability of the superconducting properties are desired. Low costs are not only related to the material manufacturing, but also to the operating conditions, e.g., the number of broken elements during production, transport, installation and operation. It is therefore necessary to produce highly reliable structural materials, something that is only possible if a good knowledge of the relationship between the properties and the microstructure of these materials is provided.

In the literature there are some works about the mechanical properties of these materials at low temperature, where their mechanical properties have been studied partially by different methods but mainly by indentation [9,10]. Unfortunately the indentation and nanoindentation mechanical measurements are quite local and not completely representative of the macroscopic structural behavior of the material, since the indentation size is similar to the microstructural size of the material. Additionally, in most of the papers only one or two types of tests are performed in materials produced by only one route [11,12]. In this contribution the mechanical behavior at 300 and 77 K (by immersion in liquid nitrogen), of two HTSC bulk materials of YBaCuO (sintered by two different methods) is thoroughly and critically examined, by using macroscopical and microscopical mechanical tests. The fracture and deformation micromechanisms have been also carefully analyzed for each testing condition. The comparison between both materials has been performed in order to get a whole understanding of the influence of the main sintering methods in the macroscopic mechanical behavior of them.

2. Experimental procedure

The studied materials involved two different methods. The first one was manufactured by the top-seeded melt growth (TSMG) method, a well-known process for growth of large grains of Y–Ba–Cu–O [13], and the second by means of the Bridgman method. The fabrication processes are described in detail below.

2.1. Sintering process

YBaCuO powders were prepared by the polyvinyl alcohol (PVA) method [14]. The used ratio 69% (w/w) Y-123, 30% (w/w) Y-211 and 1% (w/w) $CeO_2 \cdot H_2O$ was chosen to maximize critical current density [15]. The standard composition of the starting material was Y-123 with an excess of 30% (w/w) Y-211. $CeO_2 \cdot H_2O$ was added to improve the distribution of Y-211 particles. The calcined powder was deagglomerated by ball milling in an agate mortar. Green bulk pieces were obtained by cold isostatic pressure (CIP).

2.2. Texturization process

2.2.1. Top-seeded melt growth technique (TSMG)

A seed of $NdBa_2Cu_3O_{7-\delta}$ was used as pioneer at a temperature below the peritectic temperature of YBaCuO material, ($T_p = 1010\ ^\circ C$) [16]. The reaction that was carried out is a peritectic reaction where the progress of YBaCuO growth starts from a forehead growth of Ba and Cu ($BaCuO_2 + CuO$) and a solid stage, Y-211 [17], in order to obtain a crystal. From now on this material will be denoted as Y-TSMG.

2.2.2. Bridgman technique

A sample of a cylindrical shape was displaced through a thermal gradient, from a higher temperature than the T_p to a lower one. A solid–liquid interface that produces the directional growth through the cylinder was established. The crystal growth occurs via a competition process between the nucleated grains on the warmer edge of the cylinder (polydomain zone) [18]. From now on this material will be denoted as Y-Bridgman.

2.3. Oxygenation process

The oxygenation process was achieved in the samples by using a kiln with a 99.9% pure oxygen flow, at 0.4 l/min, during 240 h at 450 °C [14]. In this stage the oxygen diffuses from the surface of the material to the inside, in order to transform the material from the not superconducting tetragonal phase to the orthorhombic one (superconducting). During this process, the highest amount of micro-cracks in the material is produced, due to the difference in the microstructure lattice parameter between the two structures [7,19,20]. For this reason, the oxygenation process is of critical importance and should be performed in a particularly careful manner.

2.4. Preparation of bulk YBaCuO samples for testing

Prismatic specimens of $6 \times 5\ mm^2$ in section and between 10 and 20 mm in length were obtained through the TSMG method. All the samples were embedded in epoxy resin to enable cutting them in smaller prisms suitable for mechanical characterization. From each prismatic specimen a longitudinal cut allowed the acquisition of four samples with nominal sections of $2.0 \times 1.6\ mm^2$. In order to remove the epoxy resin, the embedded samples were heated at 400 °C in air atmosphere for 30 min.

The samples manufactured through the Bridgman method were cylindrical-shaped bars with nominal dimensions of 6 mm

in diameter and between 15 and 30 mm in length. Because of the limited quantity of material, each cylinder was embedded in epoxy resin and then was cut, in order to obtain the flat surface. Then, the epoxy resin was removed by a heating at 400 °C. This process was repeated several times until prismatic samples of the desired dimensions were obtained. From these prisms two samples were obtained by using a similar process to the one used in the case of the material fabricated by the TSMG (Y-TSMG).

Finally, in order to determine the fracture toughness of these materials, a notch was machined in the central section of the beams [12] with a thin diamond wire (Well 3241, Swiss), to a notch tip radius of 65 μm. The length of the notch was nominally 30% of the thickness of the sample in all cases. Introduction of longer notches or V-notch was not considered practical, due to the small residual force necessary to break the notched specimens.

2.5. Mechanical characterization

Three-point bending tests on prismatic bars were performed to determine fracture strength and fracture toughness. In all cases the span between supports was 8.5 and 16.0 mm, depending on the sample dimensions after the mechanizing process.

In the case of the first material (Y-TSMG), both tests were performed in the two directions (Fig. 1 *Direction T1* = the applied load was perpendicular to the *ab*-plane and *Direction T2* = the applied load was parallel to the *ab*-plane) to study the effect of the microstructural anisotropy on the mechanical properties. In the case of the second material, (Y-Bridgman) the tests were performed in a single direction, because of the radial microstructural isotropy of the material. All tests were carried out in a servohydraulic machine, (Instron 8501 USA), where the applied load and the displacement of the loading point were recorded constantly during the test with a load cell of 100 N ± 1 N and a linear variable differential transductor (LVDT) of ± 1 mm of displacement range (± 1 μm resolution).

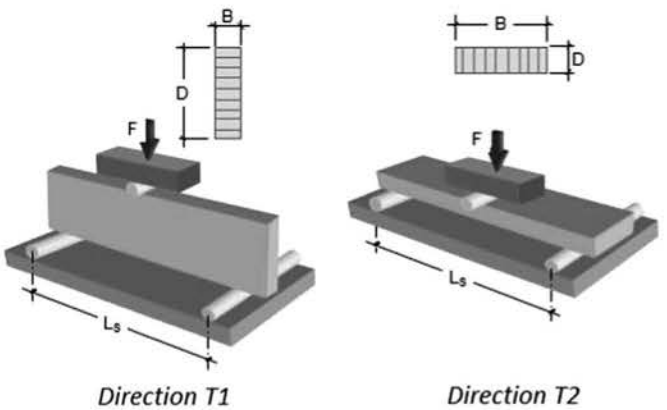

Fig. 1. Sketch where the two applied test directions for Y-TSMG can be observed. The fine bars in the cross section mark the direction of the cracks parallel to the *ab*-plane.

The test device used at low and room temperature was similar in each case. The main difference between the two cases was that at low temperature tests an additional cryogenic chamber was attached to the servohydraulic machine to the load direction. The bottom of the vessel and its load application point were connected with the actuator and the load cell of the machine, respectively, through hollow bars of stainless steel to prevent excessive cooling of the measurement devices. The chamber was coated with polyurethane to insulate the system and keep the temperature constant during the experiments. Cryogenic tests were performed by immersion of specimen in liquid nitrogen. Temperature was stabilized before each test. During the test, the liquid nitrogen level in the cryogenic vessel was maintained almost constant by refilling it when it was necessary to maintain the specimen completely immersed. As it could be monitored, this process did not affect either the measurement of the load or the displacement.

Prior to the cooling process, all the testing devices and specimen were fixed and a constant low value of load (5 N) was applied to keep the system in balance and avoid any movement of the sample or the supporting rollers during the freezing. The three-point bending tests were performed using displacement control at a constant cross-head speed of 100 μm/min.

Flexural strength was computed from the maximum load using the classic equations of strength of materials [21], while the fracture toughness was calculated by the maximum load and the post-mortem notch length using the equation developed by Guinea et al. [22].

The Vickers and nano hardness for both materials at 300 K were also studied and the tests performed for both transversal and longitudinal sections. In the case of the Vickers tests, a hardness tester (AKASHI, MVK-EIII) was used with loads of 0.98 N and 9.80 N applied for 15 s. The test was repeated 10 times for each test condition in order to obtain statistical significance.

The Vickers hardness was also measured at service temperature (77 K) for both materials. For this kind of test, it was necessary to develop a new device in order to fix the sample during both the immersion in liquid nitrogen and the subsequent indentation.

The nano hardness of both materials was measured by nanoindentation tests (MTS Nano Indenter, CSM/LFM Control Unit), using a calibrated Berkovich tip indenter [23]. In all cases, the depth of the indentation was constant ($h = 1$ μm) and the applied load varied from 130 and 160 mN. The tests were carried out for the longitudinal and transversal section.

After testing all the samples, their surfaces were analyzed with a scanning electron microscope SEM (JEOL 6130, Japan) with X-ray microanalysis, in order to find the micro-mechanisms responsible for the macroscopically mechanical behavior of these materials.

3. Results and discussion

3.1. Microstructural analysis

Both materials were characterized microstructurally with the aim of linking microstructural variations with the changes in

the mechanical properties and the fracture behavior. To prepare the specimens for SEM observation, both the transversal and longitudinal sections of each material were embedded in epoxy resin and then sequentially polished up to 1 μm. After this polishing process, the polished surfaces were etched with a solution of 95% of 2-butoxietanol and 5% of percloric acid, at 273 K for 1–1.5 min depending on the material (Y-TSMG and Y-Bridgman) to reveal their microstructure. The microstructure was studied for both materials by SEM and optical microscopy.

In both cases (Y-TSMG and Y-Bridgman) a heterogeneous distribution of the secondary phase, Y_2BaCuO_5 (Y-211), which had not reacted during the peritectic reaction Liquid + Y-211 → Y-123 could be observed (small zones with rectangular or round shape). This phenomenon is more noticeable in the case of Y-Bridgman, producing a denser superconducting grain, because the particles of Y-211 typically improve the growth of the crystal and by preventing the liquid flow, the amount and size of the pores could decrease. [24]. Also, the heterogeneous distribution of fine Y-211 particles in Y-123 matrix acts as pinning centers under superconducting conditions and increases the current density of the material [15]. In addition, according to Fig. 2, it can be observed that in the structure of the Y-TSMG superconducting domain during the oxygenation process cracks form smaller and narrower areas than that in the case of the Y-Bridgman domain. Micro- and macro-cracking for both materials were also observed, respectively, during the oxygenation and the texturization processes [7]. Microcracking was due to the different oxygen diffusion coefficients between the crystallographic planes whereas macro-cracking is caused by the different thermal expansion coefficients of the Y-211 and Y-123 phases [25].

3.2. *Flexural strength*

At least five tests were carried out for each material, microstructural direction and test temperature. In all cases, linear elastic brittle fracture was observed both at room and low temperature. The obtained flexural strength is shown in Fig. 3. This figure shows that Y-TSMG samples tested with the crystallographic *ab*-planes perpendicular to the applied load direction (*T*1 direction) presented a value of the strength, σ_f, 40% lower than the value obtained with the crystallographic *ab*-planes parallel to the applied load direction (T2 direction). Y-Bridgman samples tested at 300 K exhibited the same flexural strength as the Y-TSMG in T2 direction.

At 77 K the mean value of the flexural strength increased, achieving a value that was almost twice the value of Y-TSMG at the same temperature. When the test was carried out at 77 K, the flexural strength provided equal results for each direction. This effect, according to the literature [26–27], takes place due to the formation of thin ice layers over the surface of the specimen during the cooling process, from pre-existing ambient humidity. These ice layers partially covered the surface of pre-existing defects on the specimen surface, hence decreasing the critical size of the flaw and rounding its initial superficial tip radius.

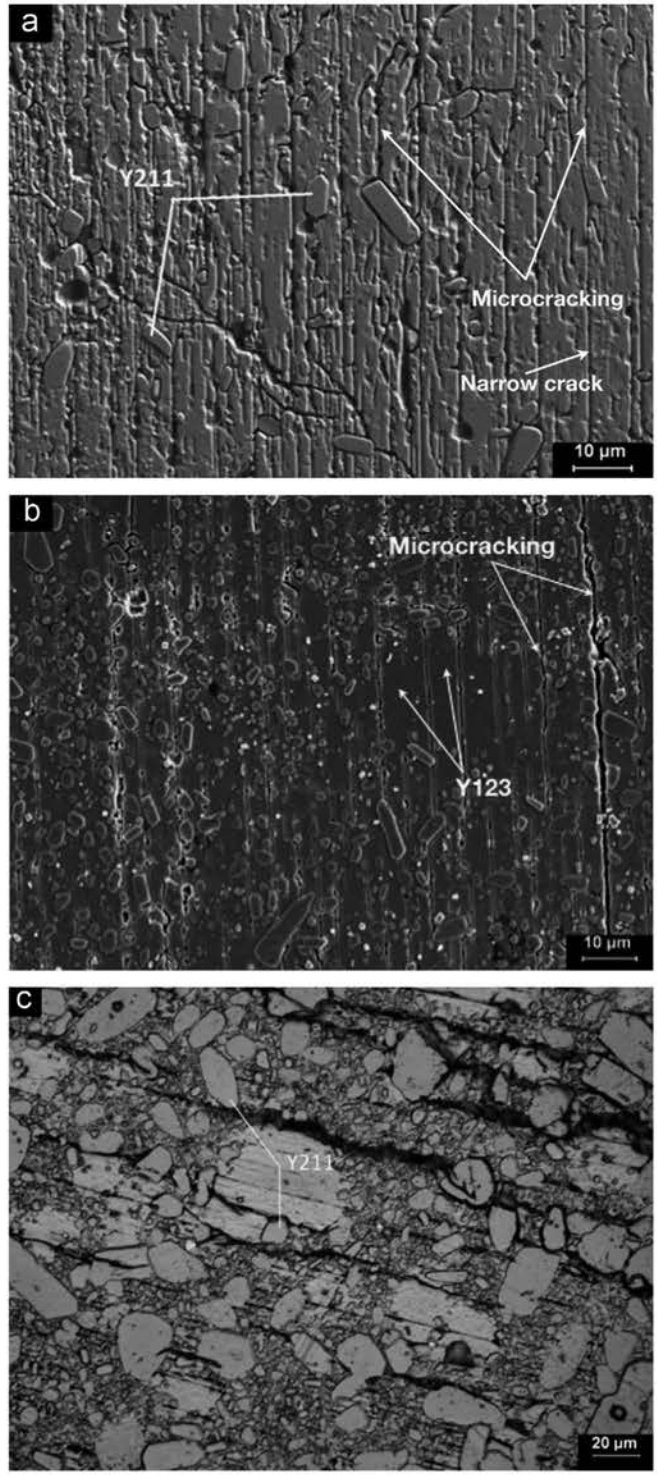

Fig. 2. (a) Microstructure of the longitudinal section Y-TSMG. This picture was obtained through electronic microscopy and presents the crack propagation perpendicular to the *ab*-planes (b) microstructure of the longitudinal section Y-Bridgman. It presents the crack propagation parallel to the *ab*-planes, and (c) microstructure of the transversal section for Y-Bridgman. The picture presents the density of cracking and the Y-211 particle size.

This effect is also observed in other porous materials like concrete; during cooling, water vapor from the atmosphere condensates and produces a gradual sealing of the pores or a reduction in their size [27–30]. Consequently, a smaller

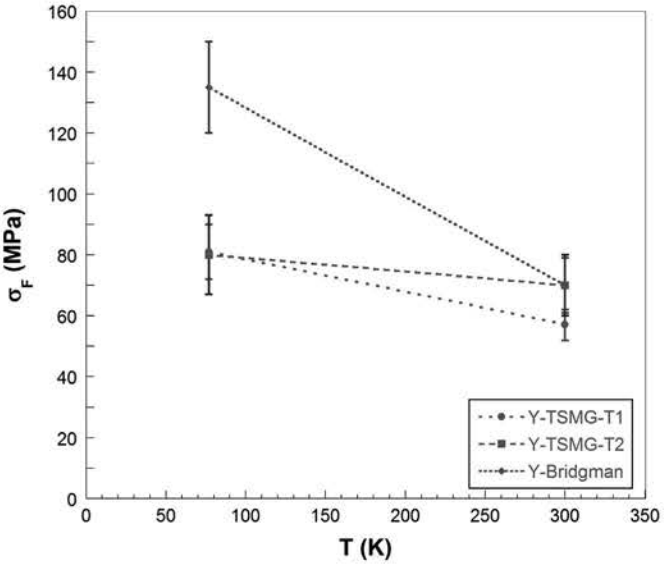

Fig. 3. Evolution of the flexural strength in function of the temperature, test direction and fabrication method. Each point presents the value of the mean of at least five tests and the bars indicate the quadratic mean error.

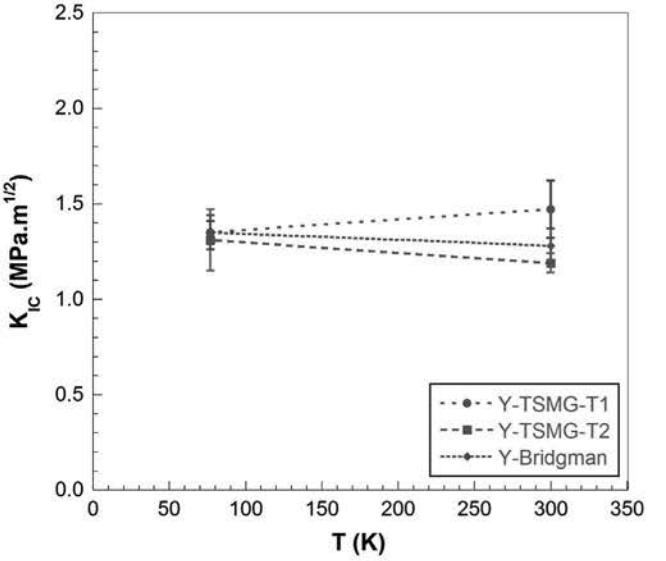

Fig. 4. Evolution of the fracture toughness in function of the temperature, test direction and fabrication method. Each point presents the value of the mean of at least five tests and the bars indicate the quadratic mean error.

superficial flaw tip radius arises, that reduce significantly the local stress intensity factor, and as a result higher flexural strength of the material is necessary for material failure.

This is a plausible explanation for the mechanical behavior of the Y-TSMG material at low temperature when the value of the flexural strength converges to the same result for both test directions. In the case of Y-Bridgman, the smaller pore, size and geometry, made this mechanism more effective, producing therefore a marked increase of the flexural strength.

3.3. Fracture toughness

To determine the fracture toughness, for both materials, at least five tests were performed for any possible microstructural direction and temperature. In all cases brittle fracture was observed, with the obtained results of the fracture toughness, K_{1c}, being presented in Fig. 4. As can be observed, Y-TSMG samples tested in the *T*1 direction presented the higher value of fracture toughness at 300 K.

In contrast, the Y-Bridgman at 300 K exhibited almost the same fracture toughness value as Y-TSMG in the T2 direction and fracture toughness increased at 77 K. On the other hand, Y-TSMG in th *T*1 direction presents a slight decrease of the toughness value at 77 K.

3.4. Fractography

SEM characterization of the fracture surfaces was performed for each specimen tested. As can be observed in Fig. 5, both materials exhibited an appreciable amount of porosity, with a considerable size. The main difference between them was the different size of pores, greater for Y-TSMG and significantly smaller, though in a larger amount, for the Y-Bridgman. In addition, it was observed that materials obtained by both methods were not perfectly sintered. These poorly-sintered zones (cavity) (Fig. 5c) could be responsible of the observed porosity in both materials.

The fracture surfaces of both materials were in all cases typically brittle, with macroscopically flat fracture surfaces and at the microscopically level fractures due to cleavage processes (Figs. 6–8). No dependence on the material, the temperature or test direction was found. In addition, it can be observed that in the case of Y-TSMG material, in the direction *T*1, the fracture surface was macroscopically flatter than in the *T*2 direction, where several discontinuities were observed in the fracture surface. Conversely, the fracture surface of the Y-Bridgman (Figs. 7,8) was rough, more similar to that of the Y-TSMG in the *T*2 direction than that of the *T*1 direction. It can also be observed that during the three-point bending tests in the Y-Bridgman, as well as in the Y-TSMG in the *T*2 direction, several cracks propagated in the perpendicular direction to the plane of the main crack propagation (Fig. 7). This local ramification of the crack front resulted in an increase of the energy and the flexural strength of the material, as was observed. In the case of Y-Bridgman, more cavities and voids were found in the fracture path, which contributed in enhancing grain boundary decohesion. Such an effect was probably responsible for the lower value of fracture toughness observed in the case of the material examined under the Bridgman technique. It was observed that in the case of Y-Bridgman and Y-TSMG in the *T*2 direction, the fracture was mainly controlled by the density of cracking. In the case of the material Y-TSMG in the *T*1 direction, the fracture was mainly controlled by the fracture of the areas between cracks (propagation of the crack perpendicular to the *ab*-plane). For this reason, and considering the small and narrow areas produced due to microcracking on the Y-Bridgman and Y-TSMG domains, the propagation of the crack happened more easily through the pre-existed microcracks than perpendicular to the *ab*-planes. This result explained the lower value

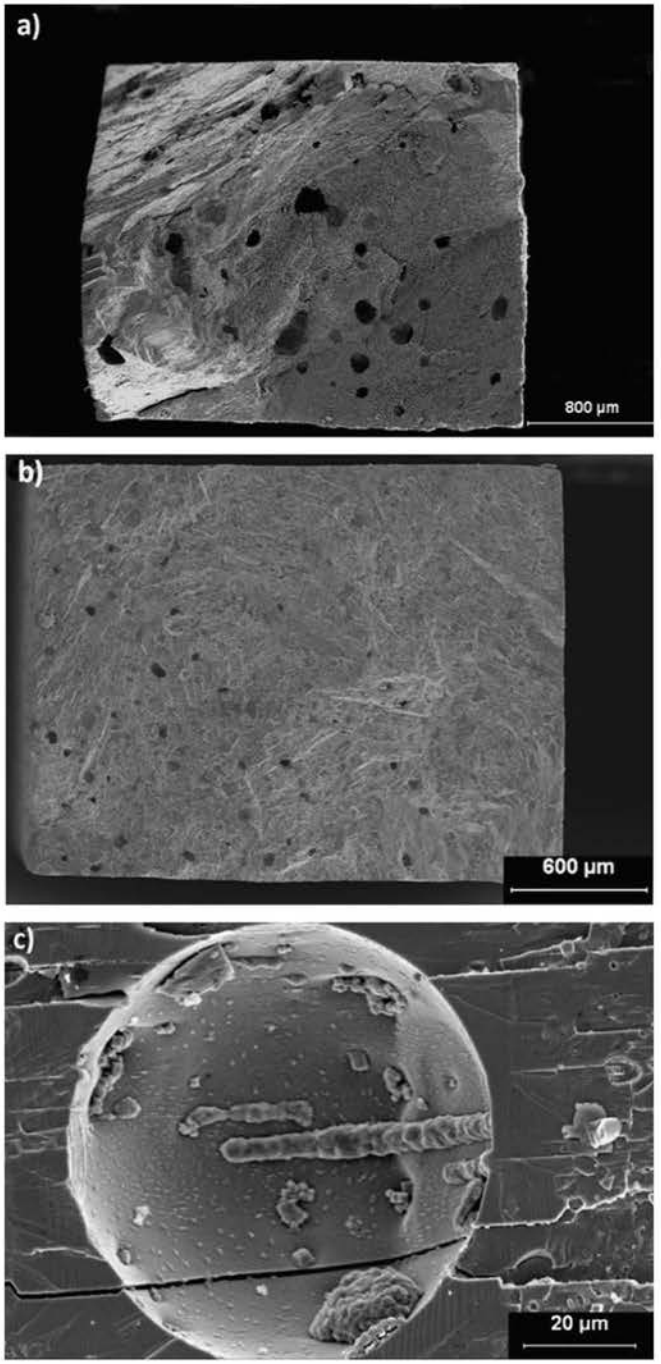

Fig. 5. Fracture surfaces at 77 K of (a) Y-TSMG, *T*2 direction. The figure presents the quantity and the large porous. (b) Y-Bridgman. The figure presents the more quantity of porosity and the smaller size of porous and (c) Y-TSMG in the *T*1 direction. This figure presents the inside part of a cavity, where there is the remainder of the bad sintering that has produced a void.

of the fracture toughness for the Y-Bridgman and Y-TSMG in the *T*2 direction at 300 K.

However, with the reduction of the temperature (77 K), a slight decrease of the fracture toughness was registered for the material Y-TSMG in the *T*1 direction. This could occur due to the embrittlement of the superconducting domain as the testing temperature decreased. This small effect is not relevant for the other conditions, where the microcracks control the fracture

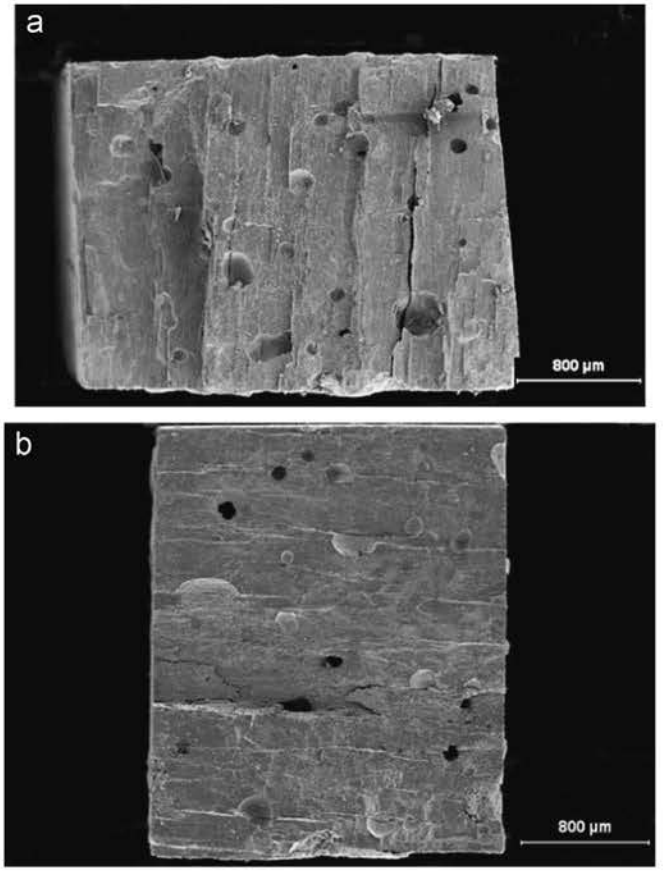

Fig. 6. Fracture surfaces at 77 K of (a) Y-TSMG in the *T*2 direction, and (b) Y-TSMG in the *T*1 direction. Brittle fracture and macroscopically plane.

process. In fact, the size of the microcracks can improve at low temperature due to the increase of thermal stresses.

3.5. Vickers and nano hardness test

The load and microstructural orientation effect were studied for both materials (Table 1). In the case of Y-TSMG at 300 K the Vickers hardness presented an almost constant value for the transversal section, as well for the longitudinal one, regardless of the applied load. In contrast, the Y-Bridgman exhibited a higher hardness in the transversal section than in the longitudinal one. In addition, the difference between the hardness of the two sections was maintained with an increasing applied load. The value of the Vickers hardness of theY-TSMG was higher than that of the Y-Bridgman in all cases at 300 K, probably due to a lower porosity level and the narrower cracks of its microstructure. On the contrary, the value of the nanohardness was higher for the material Y-Bridgman and for both materials it could be observed an increase of the nano hardness for the transversal sections. At this point it should be noted that in the case of the Vickers hardness test, the load was applied on an extended zone of the surface of the material and consequently, the hardness corresponded to a large area of the superconducting domain including some defects. Conversely, in the case of the nano hardness test, the load was extremely small and as a result the size of the mark of the Berkovich tip

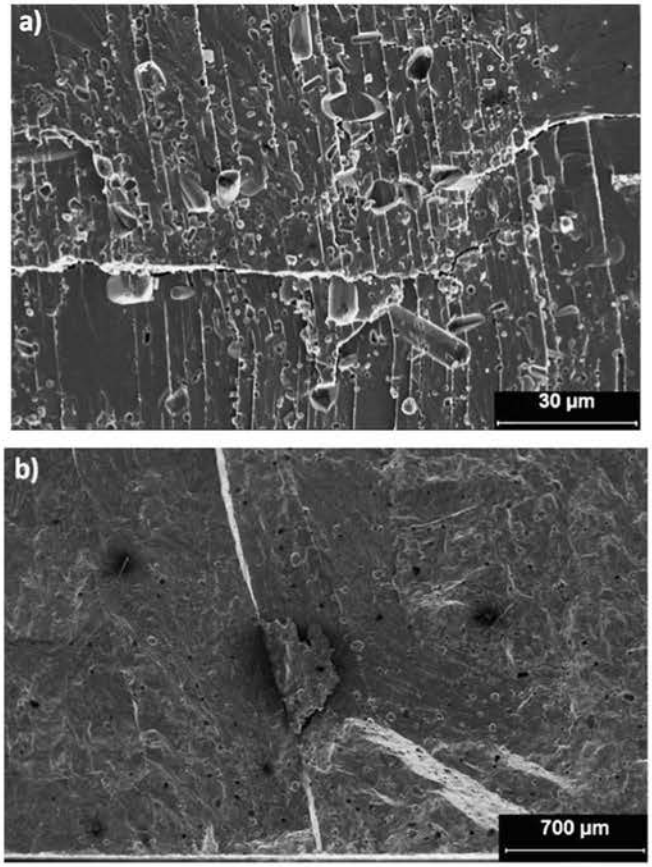

Fig. 7. Fracture surfaces at 300 K of (a) Y-TSMG in the *T*2 direction. It presents a fracture surface where a change in plane of the fracture can be observed, and (b) Y-Bridgman where a perpendicular crack to the fracture surface, produced during the fracture process, can be observed.

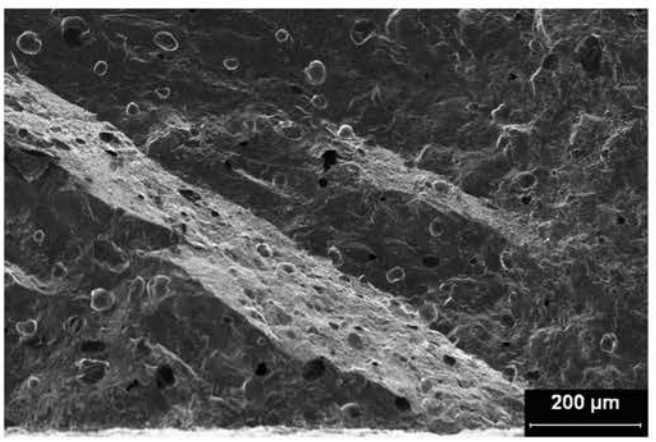

Fig. 8. Fracture surface of Y-Bridgman at 300 K. This figure presents the porosity and the smaller size of pore.

was one order of magnitude smaller than the distance between the microcracks. Hence nanoindentation allowed the hardness of individual areas of the compound YBaCuO to be determined, while in the case of Vickers hardness the global microstructure of the material was characterized (defects, porosity, microcracks, amongst others). For this reason, it could be inferred that in the case of Y-TSMG narrower cracks parallel to the *ab*-plane have been observed than in the case of the Y-Bridgman, although the second presented more compact areas between cracking in the structure of the superconducting domain. This offered a significant degree of agreement with the results shown in previous sections. Thus, in spite of the fact that the results of both tests were different, they do provide complementary information about these materials.

Additionally, for both the Y-TSMG and Y-Bridgman, Vickers hardness decreases when higher loads were applied. This effect was a consequence of the increase in the damage introduced in the material with the higher loads; when force was increased, irreversible deformation grew in a linear way due to the presence of porosity together with the delamination and fracture of the grain.

Hardness tests at 77 K (Table 2) showed that the value of the hardness increased at low temperature for both materials in a highly relevant proportion (around 50%). However, in this case the value of the Vickers hardness of Y-TSMG was smaller than that of the Y-Bridgman, inverting the situation from room temperature. This effect could be explained again by the formation of superficial ice layers during cooling. As this effect became more intense as the pore size decreased, it contributed to a greater extent to increase the low temperature hardness of the Y-Bridgman.

Finally, the postmortem surface of each material was studied by means of scanning electron and optical microscopy. Fig. 9 shows the typical propagation of the cracks on the material surface. It could be observed how the cracks were preferentially propagated parallel to the *ab*-planes. Furthermore, when a crack was forced to grow perpendicularly to the *ab*-planes, it was quickly impelled by the microstructure to turn towards a direction parallel to the *ab*-plane. Due to the irregular pattern of cracks (consequence of the anisotropic microstructure) it was not possible to determine the fracture toughness by this method. Additionally, those regions with a greater proportion of Y-211 presented crack deflections, because the propagation of the cracks occurred preferentially around and not through them because the Y-211 phase was tougher than the Y-123 one [7,31].

3.6. Critical size of defect "α"

Once the mechanical tests for both materials had been performed, the critical size "α" of a semi-elliptical defect in a flexural strength tests was calculated as a function of the fracture toughness (K_{1C}) and the flexural strength (σ_f) for each material, direction and test temperature. The obtained results, as well the applied equation [32], are shown below:

$$K_{1c} = 1.29\sigma_f\sqrt{\alpha} \quad (1)$$

In Table 3, it can be observed that the calculated critical size of the defect is smaller in the case of service temperature regardless of the material and the test direction. This phenomenon was also due to the formation of the superficial ice layers, as explained previously.

As can be observed in Fig. 10, in the case of Y-TSMG the obtained results correspond approximately to an elliptic superficial size defect detected on its fracture surface both at 300 K

Table 1
Results obtained of the nano-hardness and Vickers hardness tests at 300 K. Applied load, mean value and mean quadratic error.

Material Test direction	Nano Hardness (GPa) Load 130–160 mN	Vickers Hardness (GPa) Load 0.98 N	Vickers Hardness (GPa) Load 9.8 N
Y-TSMG (longitudinal)	8.2 ± 0.2	7.5 ± 0.2	5.7 ± 0.2
Y-Bridgman (longitudinal)	8.8 ± 0.2	5.4 ± 0.2	4.4 ± 0.2
Y-TSMG (transversal)	8.0 ± 0.1	7.1 ± 0.2	6.1 ± 0.1
Y-Bridgman (transversal)	9.3 ± 0.1	6.4 ± 0.2	5.5 ± 0.1

Table 2
Results obtained of Vickers hardness tests at 77 K. Applied load, mean value and mean quadratic error.

Material Test direction	Vickers Hardness (GPa) Load 0.98 N	Vickers Hardness (GPa) Load 9.8 N
Y-TSMG (longitudinal)	9.6 ± 1.0	8.1 ± 0.5
Y-Bridgman (longitudinal)	14.1 ± 2.0	12.7 ± 0.7
Y-TSMG (transversal)	10.2 ± 0.4	7.5 ± 0.1
Y-Bridgman (transversal)	14.9 ± 0.5	9.5 ± 0.2

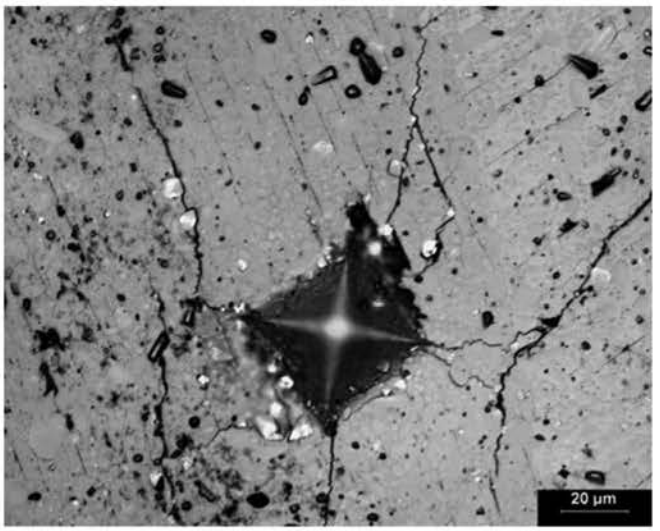

Fig. 9. Indentation on the transversal section of the material Y-Bridgman at 300 K applying load of 0.98 N.

and 77 K. The same results were obtained in the case of Y-Bridgman. The experimental results of the crack size showed good agreement with the calculated ones, which back the previous hypotheses.

From Table 3, it can be appreciated that the material Y-TSMG ($T1$ direction) presented the highest value of "α". This occurred because of the connection of the pores with the inappropriately sintered zones. Although the size of the elliptic defect was not of a notable size, the other measured defects near to the elliptic one contributed to a high value of "α". This result showed good agreement with the value of the flexural strength, which was the lowest of the materials. In contrast, the material Y-Bridgman presented at service temperature the lowest value of the size of elliptic defect, which was very close to the calculated value.

These results corroborate the crucial role of the critical defects size on the toughness and flexural strength of both materials and allow an enhanced understanding of the relationship between microstructural defects and macroscopic properties.

4. Conclusions

In this work the mechanical behavior of two second generation YBCO bulk superconductors, prepared by the TSMG and the Bridgman methods, were studied and strong correlation between the processing method, microstructure, and microscopic and macroscopic mechanical properties, at 300 and 77 K, has been found and discussed.

In the case of the TSMG material, the microstructure was transversely anisotropic, while for the Bridgman-manufactured one, microstructural isotropy was observed. It has been shown that this difference determines the mechanical properties of both materials. Additional to the microstructural anisotropy (Y-TSMG was tested in two directions while Y-Bridgman only in one direction), another important point to explain the mechanical behavior is the presence of porosity. In the case of the material fabricated by the TSMG, the greater size of the pores determined its poorer mechanical strength.

The properties of Y-TSMG were anisotropic, because of the microstructural anisotropy of the crystal, while the material Y-Bridgman did not show such characteristic. The fracture toughness of the material Y-TSMG ($T2$ direction) and Y-Bridgman increased at 77 K, because the fracture was controlled by the density of cracking. On the other hand, the fracture toughness of the material Y-TSMG ($T1$ direction) slightly decreased at 77 K, given the fact that the macroscopically fracture was controlled by the fracture of the superconducting domain that became a little more brittle. For both materials, it was observed that the strength improved with the decrease of temperature due to formation of superficial ice layers that reduce the critical size and tip radius of superficial flaws. Additionally, Y-TSMG showed greater hardness at macroscopic level at 300 K than Y-Bridgman due to the narrower areas in the structure of the superconducting domain. On the contrary, Y-Bridgman presented greater hardness both

Table 3
Value of the calculated critical size defect "α" on the fracture surface of the tested materials.

T (K)	Y-TSMG-T1 α (μm)	Y-TSMG-T2 α (μm)	Y-Bridgman α (μm)
300	399.9	173.7	200.9
77	166.9	161.3	60.1

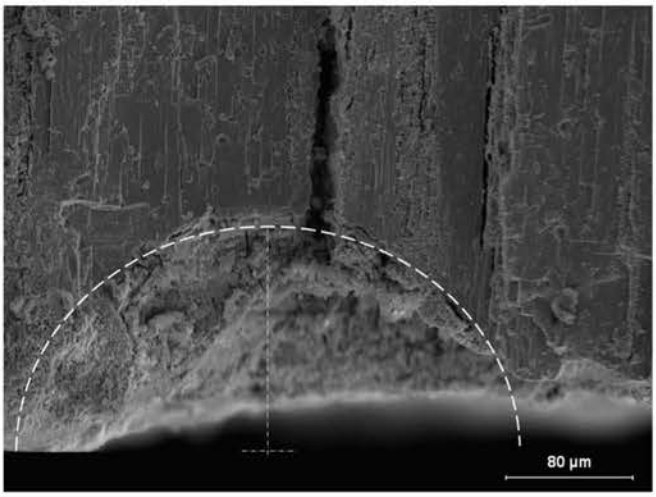

Fig. 10. Elliptic size defect on the fracture surface of Y-TSMG in the *T*2 at 77 K. The size of the defect that corresponds to the theoretical value can be observed.

at macroscopic level at 77 K and at nanoscale than Y-TSMG, because the areas between cracks were more compact and also because of the higher number of microcracks in the case of Y-TSMG.

Acknowledgments

The authors would like to acknowledge the funding for this research project of the Ministerio de Economía y Competitividad of Spain (MAT2012-38541-C02-02) and Comunidad de Madrid (S- S2009/MAT-1585). Also, they would like to thanks the support of the equipment cofounded by the CEI Campus Moncloa for the microscopy analysis at the Materials Science Department of the Technical University of Madrid.

References

[1] G. Fuchs, G. Krabbes, P. Schätzle, S. Gruß, P. Verges, K.-H. Müller, J. Fink, L. Schultz, Trapped fields larger than 11 T in bulk YBa Cu O material, IEEE Trans. Appl. Supercond. 10 (2000) 890–893.

[2] Raquel Gonzalez-Arrabal, Michael Eisterer, Harald W. Weber, Günter Fuchs, Peter Verges, Gernot Krabbes, Masaru Tomita, Masato Murakami, Doris Litzkendorf, Tobias Habisreuther, Wolfgang Gawalek, Temperature dependence of the trapped field and mechanical properties of neutron irradiated and reinforced $YBa_2Cu_3O_7$ bulk superconductors, IEEE Trans. Appl. Supercond. 13 (2) (2003) 3125.

[3] A. Salazar, J.Y. Pastor, J. Llorca, Fatigue behavior of multifilamentary BSCO 2223/Ag superconducting tapes, IEEE Trans. Appl. Supercond. 14 (3) (2004) 1941–1947.

[4] Y. Ren, R. Weinstein, J. Liu, R.P. Sawh, C. Foster, Damage caused by magnetic pressure at high trapped field in quasi-permanent magnets composed of melt-textured Y–Ba–Cu–O superconductor, Phys. C 251 (1995) 15–18.

[5] P. Diko, Growth-related microstructure of melt-grown REBaCuO bulk superconductors, Supercond. Sci. Technol 13 (2000) 1202–1213.

[6] K. Zmorayova, P. Diko, G. Krabbes, Oxygenation cracks in top seeded melt growth YBaCuO bulk superconductors, Phys. C 445-448 (2006) 436–439.

[7] J.J. Roa, F.T. Dias, M. Martinez, J.A. Padilla, M. Segarra, Oxygenation kinetics of YBCO-TSMG samples using nanoindentation technique, J. Eur. Ceram. Soc. 32 (2012) 425–431.

[8] J.J. Roa, K. Konstantopoulou, E. Jiménez-Piqué, V. Martín, M. Segarra, J.Y. Pastor, Nanoindentation of Bridgman YBCO samples, Ceram. Int. 38 (2012) 2035–2042.

[9] Y. Yoshimo, A. Iwabuchi, K. Noto, N. Sakai, M. Murakami, Vickers hardness properties of YBCO bulk superconductor at cryogenic temperatures, Phys. C Supercond. 357–360 (2001) 796–798.

[10] F. Yu, K.W. White, R. Meng, Mechanical characterization of top-seeded melt-textured $YBa_2Cu_3O_{7-\delta}$ single crystal, Phys. C 276 (1997) 295–308.

[11] K.C. Goretta, M.L. Kullberg, D. Bär, G.A. Risch, J.L. Routbort, Fracture toughness of $YBa_2Cu_3O_x$ containing Y_2BaCuO_5 and ZrO^2, Supercond. Sci. Technol. 4 (1991) 544–547.

[12] T. Okudera, A. Murakami, K. Katagiri, K. Kasaba, Y. Shoji, K. Noto, N. Sakai, M. Murakami, Fracture toughness evaluation of YBCO bulk superconductor, Phys. C 392–396 (2003) 628–633.

[13] N. Babu, K. Lida, Y. Shi, D.A. Cardwell, Processing of high performance (LRE)-Ba-Cu-O large, single-grain bulk superconductors in air, Phys. C 445–448 (2006) 286–290.

[14] I.G. Serradilla, A. Calleja, X.G. Capdevila, M. Segarra, E. Mendoza, J. Teva, X. Granados, X. Obradors, F. Espiell, Syntering the Y-123/Y-211 composite by the PVA method, Supercond. Sci. Technol. 15 (2002) 566–571.

[15] S. Piñol, V. Gomis, B. Martinez, A. Labarta, J. Fontcuberta, X. Obradors, Bridgman growth and enhanced critical currents in textured yttrium barium copper oxide, J. Alloys Compd. 11 (1993) 195.

[16] T. Asalage, K. Keefer, Liquidus relations in Y–Ba–Cu oxides, J. Mater. Res. 3 (1988) 1279–1291.

[17] M.P. Delamare, H. Walter, B. Bringmann, A. Leenders, H.C. Freyhardt, Characterization of natural and artificial low-angle boundaries in YBCO TSMG samples, Phys. C: Supercond. Appl. 329 (2000) 160–177.

[18] X. Granados, S. Piñol, B. Martín, J. Fontcuberta, F. Sandiumenge, Procedimiento de obtención de cerámicas superconductoras texturadas de $TRBa_2Cu_3O$ donde TR significa Tierra Rara o Ytrio mediante solidificación direccional, Spanish Patent Specification 2111435.

[19] R.J. Cava, A.W. Hewat, E.A. Hewat, B. Batlogg, M. Marezio, K.M. Rabe, J.J. Krajewski, W.F. Peck, L.W. Rupp, Structural anomalies, oxygen ordering and superconductivity deficient barium yttrium copper oxide ($Ba_2YCu_3O_x$), Phys. C: Supercond. Appl. 165 (5-6) (1990) 419–433.

[20] S.J. Rothman, J.L. Routbort, U. Welp, J.E. Bajer, Anisotropy of oxygen tracer diffusion in single crystal yttrium barium copper oxide ($YBa_2Cu_3O_{7-\delta}$), Phys. Rev. B: Condens. Matter Mater. Phys. 44 (1991) 2326–2333.

[21] S. Timoshenko, Strength of Materials, 3rd ed., D. Van Nostrand Company, New York, 1955.

[22] G. Guinea, J.Y. Pastor, J. Planas, M. Elices, Stress intensity factor, compliance and CMOD for a general three-point-bend beam, Int. J. Fract. 89 (1998) 103–116.

[23] W.C. Oliver, G.M. Pharr, An improved technique for determining hardness and elastic modulus using load and displacement sensing indentation experiments, J. Mater. Res. 7 (1992) 1564–1583.

[24] J.J. Roa, E. Jiménez-Piqué, X.G. Capdevila, M. Segarra, Nanoindentation with spherical tips of single crystals of YBCO textured by the Bridgman technique: determination of indentation stress–strain curves, J. Eur. Ceram. Soc. 30 (2010) 1477–1482.

[25] F. Sandiumenge, S. Piñol, X. Obradors, E. Snoeck, C. Roucau, Microstructure of directionally solidified high-critical current $YBa_2Cu_3O_7$ – Y_2BaCuO_5 composites, Phys. Rev. B 50 (1994) 7032–7045.

[26] C. Rocco, J. Planas, G.V. Guinea, M. Elices, Fracture properties of concrete in cryogenic conditions, Fract. Mech. Concr. Struct., Sets Zeitlinger (2001) 411–416.

[27] J. Planas, P. Maturana, G.V. Guinea, M. Elices, Advances in Fracture Research ICF7, Pergamon Press, Oxford, 1989.

[28] J.Y. Pastor, P. Poza, J. Llorca, Mechanical properties of textured $Bi_2Sr_2CaCu_2O_{8+\delta}$ high-temperature superconductors, J. Am. Ceram. Soc. 82 (11) (1999) 3139–3144.

[29] A. Salazar, J.Y. Pastor, J. Llorca, Strength and fracture toughness of hot-pressed bulk $Bi_2Sr_2Ca_2Cu_3O_x$ and $Bi_2Sr_2Ca_2Cu_3O_x$/Ag at 77 and 300 K, Phys. C-Supercond. Appl. 385 (3) (2003) 404–414.

[30] A. Salazar, J.Y. Pastor, J. Llorca, E. Natividad, F.J. Gimeno, L. A. Angurel, Effect of thermal cycling on the strength and superconducting properties of laser floating zone textured Bi-2212 rods, Phys. C-Supercond. Appl. 384 (4) (2003) 443–450.

[31] J.J. Roa, X.G. Capdevila, M. Martinez, F. Espiell, M. Segarra, Nanohardness and Young's modulus of YBCO samples textured by the Bridgman technique, Nanotechnology 18 (2007) 385701/1–385701/6.

[32] Lawn Brian, in: Fracture of Brittle Solids (Cambridge Solid State Science Series), Second Ed., 1993.